Earth and Planetary Science Letters 446 (2016) 89–99

Contents lists available at ScienceDirect

Earth and Planetary Science Letters

www.elsevier.com/locate/epsl

Continental flood basalt weathering as a trigger for Neoproterozoic Snowball Earth

Grant M. Cox [a,b,*], Galen P. Halverson [a,b], Ross K. Stevenson [c], Michelle Vokaty [a], André Poirier [c], Marcus Kunzmann [a], Zheng-Xiang Li [b], Steven W. Denyszyn [d], Justin V. Strauss [e], Francis A. Macdonald [f]

[a] Department of Earth and Planetary Sciences, McGill University, Montréal, Québec, Canada
[b] ARC Centre of Excellence for Core to Crust Fluid Systems and The Institute for Geoscience Research, Department of Applied Geology, Curtin University, WA, Australia
[c] Département des sciences de la Terre et de l'atmosphère/Geotop, Université du Québec à Montréal, Montréal, Québec, Canada
[d] School of Earth and Environment/Centre for Exploration Targeting, The University of Western Australia, Crawley, WA, Australia
[e] Department of Earth Sciences, Dartmouth College, HB6105 Fairchild Hall, Hanover, NH 03755, USA
[f] Department of Earth and Planetary Sciences, Harvard University, Cambridge, MA, USA

ARTICLE INFO

Article history:
Received 22 November 2015
Received in revised form 11 April 2016
Accepted 15 April 2016
Available online 12 May 2016
Editor: M. Frank

Keywords:
Snowball Earth
cryogenian
continental flood basalts
silicate weathering
large igneous province

ABSTRACT

Atmospheric CO_2 levels and global climate are regulated on geological timescales by the silicate weathering feedback. However, this thermostat has failed multiple times in Earth's history, most spectacularly during the Cryogenian (c. 720–635 Ma) Snowball Earth episodes. The unique middle Neoproterozoic paleogeography of a rifting, low-latitude, supercontinent likely favored a globally cool climate due to the influence of the silicate weathering feedback and planetary albedo. Under these primed conditions, the emplacement and weathering of extensive continental flood basalt provinces may have provided the final trigger for runaway global glaciation. Weathering of continental flood basalts may have also contributed to the characteristically high carbon isotope ratios ($\delta^{13}C$) of Neoproterozoic seawater due to their elevated P contents. In order to test these hypotheses, we have compiled new and previously published Neoproterozoic Nd isotope data from mudstones in northern Rodinia (North America, Australia, Svalbard, and South China) and Sr isotope data from carbonate rocks. The Nd isotope data are used to model the mafic detrital input into sedimentary basins in northern Rodinia. The results reveal a dominant contribution from continental flood basalt weathering during the ca. 130 m.y. preceding the onset of Cryogenian glaciation, followed by a precipitous decline afterwards. These data are mirrored by the Sr isotope record, which reflects the importance of chemical weathering of continental flood basalts on solute fluxes to the early–middle Neoproterozoic ocean, including a pulse of unradiogenic Sr input into the oceans just prior to the onset of Cyrogenian glaciation. Hence, our new data support the hypotheses that elevated rates of flood basalt weathering contributed to both the high average $\delta^{13}C$ of seawater in the Neoproterozoic and to the initiation of the first (Sturtian) Snowball Earth.

1. Introduction

The Neoproterozoic Era (1000–541 Ma) began with the amalgamation of the supercontinent Rodinia and ended with the assembly of Gondwana. Intervening global glaciations, massive perturbations to the carbon cycle, eukaryotic diversification, and presumed oxygenation of the atmosphere and ocean are broadly coincident with the fragmentation of Rodinia (Hoffman et al., 1998; Condon et al., 2005; Swanson-Hysell et al., 2010; Li et al., 2013). Mechanistic interconnections among these events are commonly invoked, but remain conjectural. Middle Neoproterozoic paleogeography (Fig. 1) likely favored both a cool global climate and elevated burial rates of organic carbon (Swanson-Hysell et al., 2010), as evinced in unusually high (~ 5‰) average carbon isotope compositions of marine carbonates ($\delta^{13}C_{carb}$) at this time (Fig. 2). Horton (2015) recently proposed that the high $\delta^{13}C_{carb}$ values were driven by the weathering of extensive large igneous provinces (LIP's) during the Neoproterozoic, which would have greatly increased riverine phosphorus fluxes to the global ocean.

* Corresponding author at: ARC Centre of Excellence for Core to Crust Fluid Systems and The Institute for Geoscience Research, Department of Applied Geology, Curtin University, WA, Australia.
E-mail address: grant.cox@curtin.edu.au (G.M. Cox).

http://dx.doi.org/10.1016/j.epsl.2016.04.016
0012-821X/

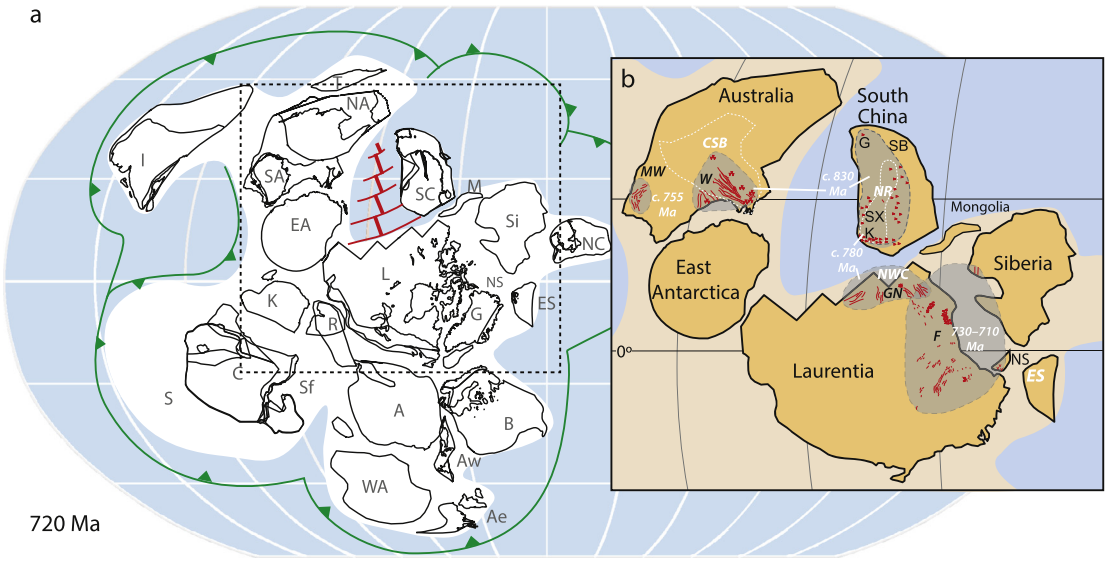

Fig. 1. Paleogeographic reconstruction for Rodinia at 720 Ma and distribution of early Neoproterozoic LIP's in northern Rodinia. a) Paleogeography of Rodinia modified from Li et al. (2013). I = India; SA = southern Australia; NA = northern Australia; T = Tarim; SC = South China; M = Mongolia; EA = East Antarctica; Si = Siberia; NC = North China; L = Laurentia; NS = North Slope; ES = East Svalbard; G = Greenland; B = Baltica; A = Amazonia; WA = West Africa; Aw = western Avalonia; Ae = eastern Avalonia; Sf = Sao Francisco; C = Congo; K = Kalahari; R = Rio Plata. b) Inset of what is herein referred to as northern Rodinia, showing distribution of LIP's and locations from which Nd isotope data are derived. M = Khubsugul and Zavkhan terranes of Mongolia; NS = North Slope subterrane of Arctic Alaska. Sources of Nd isotope data: CSB = Centralian Superbasin; NWC = Northwestern Canada; NR = Nanhua Rift; ES = East Svalbard. Distribution of early Neoproterozoic LIP's in red: MW = Mundine Well; W = Willouran; GN = Gunbarrel; F = Franklin; K = Kanding; SX = Suxiong-Xiaofeng; G = Guibei; SB = Shaba. (For interpretation of the references to color in this figure legend, the reader is referred to the web version of this article.)

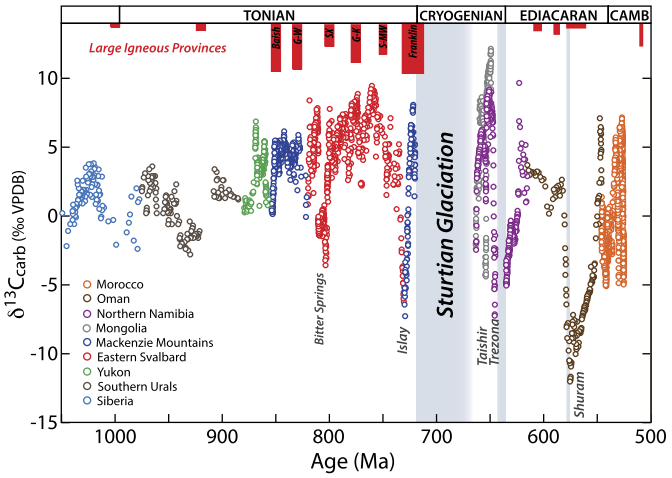

Fig. 2. Compilation of carbonate carbon isotope data ($\delta^{13}C_{carb}$) for the Neoproterozoic Era compared to the LIP record. This $\delta^{13}C_{carb}$ compilation is revised from previous compilations (Halverson et al., 2005, 2010). Prominent negative anomalies are labeled, including the Cryogenian Taishir anomaly, which has only been fully documented in Mongolia (Bold et al., 2016). Sources of the data: Morocco (Maloof et al., 2010); Oman (Fike et al., 2006); Namibia (Halverson et al., 2005; Swanson-Hysell et al., 2010) Svalbard (Halverson et al., 2005); Mackenzie Mountains (Halverson, 2006; Rooney et al., 2014); Yukon (Macdonald et al., 2012; previously unpublished data); Southern Urals (Kuznetsov et al., 2006), Siberia (Knoll et al., 1995; previously unpublished data); Mongolia (Macdonald et al., 2009; Bold et al., 2016). The LIP record (relative magnitude) is modified from Ernst et al. (2008). G–W = Guibei and Willouran; SX = Suxiong/Xiaofeng; G–K = Gunbarrel and Kanding.

The onset of the Sturtian Snowball Earth ca. 717 Ma (Macdonald et al., 2010) brought an end to over one billion years of non-glacial climate and a brief resumption in the deposition of iron formation. Like the subsequent Marinoan glaciation, which ended at 635 Ma (Condon et al., 2005), the Sturtian glaciation was preceded by a deep negative $\delta^{13}C_{carb}$ anomaly—the Islay excursion (Fig. 2; Strauss et al., 2014). Several triggers have been proposed for the initiation of snowball glaciations that are linked to these pre-glacial $\delta^{13}C_{carb}$ excursions, including a transient increase then abrupt decline in methane fluxes (Schrag et al., 2002) and enhanced organic export production and anaerobic remineralization (Tziperman et al., 2011). However, recent radiometric age constraints indicate that the Islay excursion preceded Sturtian glaciation by >10 Ma, implicitly decoupling it from the onset of global glaciation (Rooney et al., 2014; Strauss et al., 2014). A third and still viable hypothesis is that the onset of the Sturtian snowball glaciation was driven by accelerated uptake of CO_2 resulting from the emplacement and weathering of Neoproterozoic LIP's as the rifting supercontinent drifted into the wet tropics—the Fire and Ice hypothesis (Goddéris et al., 2003; Donnadieu et al., 2004).

Because LIP's have geochemical signatures that are distinct from average continental crust, massive weathering of their surficial carapaces, continental flood basalts, should leave a distinct imprint in the sedimentary record. For example, siliciclastic sediments deposited in basins proximal to continental flood basalts (CFB's) should record primitive Nd isotope signatures and other geochemical characteristics typical of a dominantly mafic provenance. Chemical weathering of CFB's should also influence ocean chemistry (Mills et al., 2014), for example through the input of unradiogenic Sr and Os (Taylor and Lasaga, 1999; Ravizza and Peucker-Ehrenbrink, 2003). Consequently, the hypothesis that a flare-up in LIP emplacement in the Neoproterozoic contributed to fertilization of the oceans (Horton, 2015) and triggering of Cryogenian glaciation (Goddéris et al., 2003; Rooney et al., 2014) is testable in the sedimentary record.

To test the predictions made by this hypothesis, we have compiled new and previously published Neoproterozoic Nd isotope data on mudstones from basins proximal to a cluster of early–middle Neoproterozoic LIP's in northwestern North America, Australia, South China, and Svalbard and Sr isotope ratios ($^{87}Sr/^{86}Sr$) from well preserved marine carbonates globally. These datasets are coupled to a new $\delta^{13}C_{carb}$ compilation for the Neoproterozoic. Together, the data reveal a dominant contribution of CFB weathering to both clastic and solute fluxes in the ca. 130 m.y. preceding Cryogenian glaciation, followed by a dramatic decrease afterwards. These results attest to a direct role of CFB weathering on modu-

lating the extraordinary paleoenvironmental perturbations of the Neoproterozoic Era and reveal the missing link between supercontinental break-up, high $\delta^{13}C_{carb}$, and snowball glaciation.

2. Large igneous provinces in the Neoproterozoic

Large igneous provinces result from the extrusion of $>10^6$ km^3 of mafic volcanic rocks, typically in less than a few million years. Although their geodynamic origin remains controversial (Sobolev et al., 2007; Wang et al., 2015), their association with supercontinental break-up is well established (Courtillot et al., 1999). They are also closely coupled to many Phanerozoic environmental catastrophes including mass extinctions and climatic perturbations (Wignall, 2001; Sobolev et al., 2011; Schaller et al., 2011; Blackburn et al., 2013). LIP emplacement, in particular CFB volcanism, perturbs global climate through the massive release of magmatic gases, most notably SO_2, which can drive global cooling on a timescale of years, and CO_2, which triggers global warming over 10^1–10^5 years (Sobolev et al., 2011; Schaller et al., 2011; Blackburn et al., 2013). CFB's also lower pCO_2 on longer timescales (10^5–10^7 years) through enhanced silicate weathering owing to the ~5–10 times greater weatherability of basalt compared to felsic continental crust (White and Brantley, 1995; Dessert et al., 2001). For example, long-term decline in pCO_2 likely followed the emplacement of both the ca. 66 Ma Deccan Traps (Dessert et al., 2001; Kent and Muttoni, 2013; Lefebvre et al., 2013) and the ca. 201 Ma Central Atlantic Magmatic Province (CAMP) (Schaller et al., 2012).

Multiple large Neoproterozoic CFB's were emplaced on northern Rodinia in the early–middle Neoproterozoic (ca. 850–720 Ma; Figs. 1, 2). The ca. 830 Ma Guibei and Willouran LIPs in South China and Australia are estimated to have covered a combined ~10^6 km^2, comparable in size to the end-Permian Siberian Traps (Ernst et al., 2008). Northwestern Laurentia (North America) hosts the ca. 780 Ma Gunbarrel LIP, which along with the coeval Kanding LIP in South China, covered an estimated original area of 1.6×10^6 km^2 (Ernst et al., 2008). The ca. 755 Ma Mundine Well LIP in western Australia (Wingate and Giddings, 2000) is inferred to have been relatively small (0.2×10^6 km^2), but roughly coeval LIP's are widespread elsewhere in Rodinia, including the Shaba Gabbro in South China (Ernst et al., 2008). Emplacement of the ca. 725–712 Ma Franklin LIP centered on northern Laurentia temporally overlapped the onset of Sturtian glaciation (Fig. S3) but apparently did not result in sufficient outgassing of CO_2 to prevent an albedo runaway (Nabelek et al., 2014). The Franklin LIP has been estimated at 2.2×10^6 km^2 in original area (Ernst et al., 2008), but was likely much larger given evidence for coeval mafic magmatism in northwestern Canada and Arctic Alaska (Macdonald et al., 2010; Cox et al., 2015), as well as slightly older but possibly cogenetic mafic intrusions in southwestern Siberia (Ariskin et al., 2013; Ernst et al., 2013) (Fig. 1b).

By the time the Franklin LIP was emplaced in northern Canada, northern Rodinia and its abundant CFB's were positioned in the wet tropics (Fig. 1). Combined with the incipient rifting of Rodinia at this time and the resulting exposure of more of the northern Rodinia land area to seaways, this paleogeography would have been uniquely suited to drive rapid basalt weathering. However, even though full break-up of Rodinia did not occur until the Ediacaran, LIP magmatism on the continents appears to have declined precipitously following the Franklin event (Fig. 2). Several relatively small LIP's were emplaced in the middle Ediacaran as the Iapetus Ocean opened (Ernst et al., 2008; McCausland et al., 2011), but combined with the drift of this region across the sub-tropics and towards higher latitudes (Li et al., 2013), their impact on global silicate weathering would have been minimal compared to that of the northern Rodinia LIP's leading up to the Cryogenian glaciation.

3. Method summary

Summaries of the methods used for this study are outlined below. Full details of these methods are provided in the supplementary information.

3.1. Carbon isotopes

Carbon isotope analyses were performed following conventional procedures (e.g. Halverson et al., 2010). In short, sample powders were drilled from slabs of carbonate hand samples, avoiding fractures, heterogeneities, and weathered surfaces. Aliquots of approximately 50–100 μg of the homogenized, powdered samples were analyzed via dual-inlet mass spectrometry on a Nu Instruments Perspective™ at McGill University. All data are expressed in conventional per mil (‰) notation and calibrated to the Vienna Pee Dee Belemnite (VPDB) reference standard. This new compilation can be found in Table S1 of the accompanying supplementary material.

3.2. Sm–Nd isotopes

Nd and Sm isotope ratios of mudstone, iron formation, and basalt samples were analyzed via thermal ionization mass spectrometry (TIMS) on a Thermo Triton™ mass spectrometer following standard multi-acid dissolution and anion exchange chromatography protocols at Geotop/Université du Québec à Montréal. Nd isotope ratios ($^{143}Nd/^{144}Nd$) are presented as $\varepsilon_{Nd(t)}$, where the $^{144}Nd/^{143}Nd$ ratio is normalized to CHUR as a function of age (t) and expressed in parts per ten thousand (Table S2).

3.3. Sr isotopes

Carbonates were pre-screened based on their Mg/Ca, Mn/Sr, Sr, and where possible, Rb concentrations or Rb/Sr ratios. Although generally samples with low Mg/Ca (<0.01), Mn/Sr (<0.1), and Rb/Sr (<0.1) and high Sr concentrations (>500 ppm) are optimal, the criteria are variable for each succession, with the degree of alteration a function of the initial mineralogy and post-burial history of each sample (Edwards et al., 2015). Prescreened samples were leached with ammonium acetate and then rinsed three times in MQH_2O. The calcite fraction of the samples was then dissolved in 0.5 M acetic acid. Following anion exchange chromatography, the isolated Sr fractions were measured via thermal ionization mass spectrometry (TIMS) on a Thermo Triton™ at Geotop/Université du Québec à Montréal. This data can be found in Table S3.

4. Results

4.1. C isotope compilation

The compilation of $\delta^{13}C_{carb}$ values shown in Fig. 2 is modified from previous compilations (Halverson et al., 2005, 2010), with additional data from Maloof et al. (2010) and Swanson-Hysell et al. (2010) and new data from Yukon (Macdonald et al., 2012 and this contribution), the southern Urals (Kuznetsov et al., 2006) and Siberia (Knoll et al., 1995 and this contribution), which extend the record back to the Mesoproterozoic–Neoproterozoic boundary. The age constraints for these successions, in particular in the Urals and Siberia, are very poor, but the relative ages are robust. This compilation suggests that moderate fluctuations in $\delta^{13}C$ (up to 6‰) were a feature of the earliest Neoproterozoic, but extreme ^{13}C-enrichment (>5‰) did not begin until ca. 850 Ma. Another key feature of the revised $\delta^{13}C_{carb}$ record is the clear offset (i.e. >10 m.y.) between the minima of the pre-Sturtian Islay anomaly

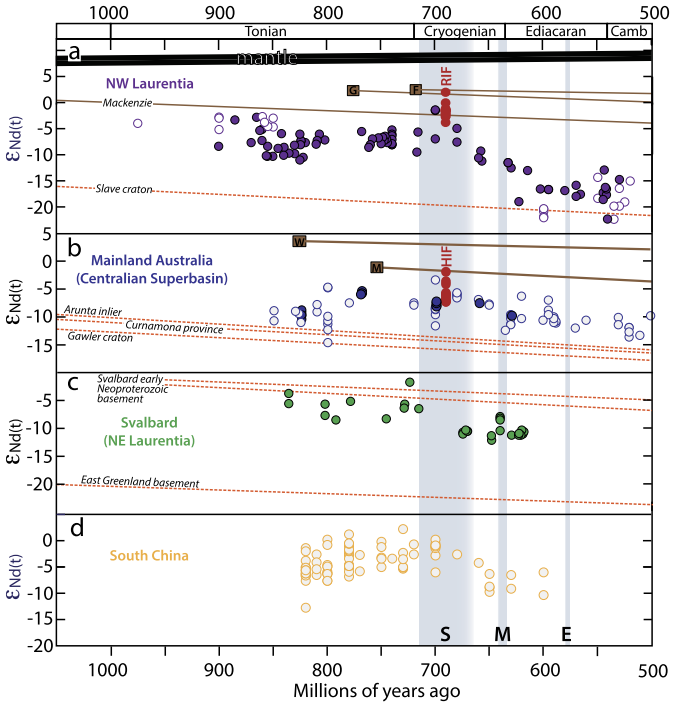

Fig. 3. Compilation of Nd isotope data from Neoproterozoic mudstones and iron formation. New data are plotted as filled circles; previously published data are plotted as light-grey filled circles. Note that for syn-glacial samples, ages are unconstrained beyond the age constrains for the glacial epoch (c. 717–663 Ma). RIF = Rapitan iron formation; HIF = Holowilena iron formation. The thick black line is the depleted mantle array. Brown lines are LIP arrays. F = Franklin; G = Gunbarrel; W = Willouran; M = Mundine Well. Dashed orange lines represent the average arrays for basement terranes for each region as calculated in this study. See Table S2 for sources of previously published data. (For interpretation of the references to color in this figure legend, the reader is referred to the web version of this article.)

and the onset of the Sturtian glaciation (Strauss et al., 2014). Indeed, the Sturtian glaciation now appears to be presaged instead by a sharp rise in $\delta^{13}C$ (from $<-5‰$ to $>5‰$).

The carbon isotope compilation is used to calibrate both the Nd and Sr isotope records, such that even if ages for individual samples are not always accurate or precise, the relative ages of the C, Nd, and Sr isotope data sets are harmonized. Age calibrations are revised from age models in Halverson et al. (2010) and Swanson-Hysell et al. (2010), with modifications based on new ages from northwest Canada (Macdonald et al., 2010; Strauss et al., 2014; Rooney et al., 2014, 2015). For each individual succession, ages between calibration points were determined, where possible, by basic thermal subsidence modeling (e.g. Halverson et al., 2002; Le Guerroué et al., 2006). Where this technique was not possible, or over short stratigraphic intervals, age models were constructed by linear interpolation between correlated ages based on the assumption of constant sediment accumulation rates.

4.2. Nd isotope compilation

Samples selected for Nd isotope analyses include mudstones, the matrices of glacial diamictite and iron formation. Our new data from North America, Australia, and Svalbard were combined with published data from North America, Australia, and South China (Table S2) to generate the four regional compilations shown in Fig. 3.

The Nd compilation from NW Laurentia displays a strikingly similar pattern to South China and Australia (Barovich and Foden, 2000; Wang et al., 2011), which together define a broad high in ε_{Nd} leading into the Cryogenian period, followed by a marked decline from the late Cryogenian to the early Palaeozoic (Fig. 3a–c). These data are consistent with Laurentia's position close to Australia and South China in northern Rodinia (Fig. 1) and highlight an extensive mafic sediment source for 130 million years preceding Sturtian glaciation. The new NW Laurentia data reveal additional detail. Specifically, ε_{Nd} is high (>-3) in the early Neoproterozoic, implying a separate source of juvenile Nd, most likely the remains of the $>2.7 \times 10^6$ km^3 Mackenzie LIP (Ernst et al., 2008) in NW Laurentia. A short-lived decline in ε_{Nd} to -10 at ca. 850 Ma likely reflects an episode of continental extension at this time that initiated early Neoproterozoic basins in NW Laurentia (Macdonald et al., 2012) and exposed fresh, evolved, continental crust. ε_{Nd} values then rise, with a culmination during the Sturtian glaciation, following Franklin magmatism. ε_{Nd} values decrease steeply following the Sturtian glaciation, reaching basement values (<-15) by the latter Ediacaran as the western margin of Laurentia fully opened (Colpron et al., 2003).

Data from mudstones in Svalbard, which lay off Laurentia (Fig. 1), also show a rise in ε_{Nd} values preceding Sturtian glaciation and an abrupt decline afterwards. These results imply a prominent juvenile source area leading into Cryogenian glaciation, consistent with an extensive Franklin LIP and our paleogeographic reconstruction (Fig. 1). The Australian Nd compilation is distinct from the Laurentian data insofar as values are close to that of Australian continental basement (~-10) in the early Neoproterozoic but rise to near zero in the matrix of Sturtian glacial deposits. This trend presumably reflects the low abundance of basalt on Australia prior to emplacement of the Willouran and possibly Guibei LIP and the dominance of basaltic provenance by the onset of the Sturtian glaciation.

We also analyzed syn-glacial iron formation (IF) in Australia and Canada, which in both cases comprise a combination of hematitic jaspilite and mudstone (Klein and Beukes, 1993; Cox et al., 2016). Samples from the Rapitan IF in NW Laurentia, which occurs within basalt clast-rich glacial deposits, show a range of relatively high ε_{Nd} (-4 to $+2$), with the most juvenile values overlapping the temporal arrays of the Gunbarrel and Franklin LIP's (Fig. 3). The Holowilena IF in South Australia has higher detrital content and displays a larger range in ε_{Nd} (-10 to -3), but still overlaps the Mundine Well LIP array (Fig. 3b). Together, these data reflect the preponderance of juvenile Nd in both the waters and sediments of the basins in which they formed.

4.3. Modeling the mafic contribution to detrital sediments (f_{maf})

To estimate the magnitude of the basaltic component of mudstone samples (f_{maf} = fraction derived from CFB), a mixing lattice was constructed utilizing the measured Nd concentrations and initial Nd isotope ratios ($^{143}Nd/^{144}Nd_{(i)}$) of local LIP's and cratonic basement (Fig. 4). For these calculations, we combined data from northwestern Canada and Svalbard to construct a single northern Laurentia dataset. Neoproterozoic LIP's show a relatively restricted range in ε_{Nd} and [Nd], especially when compared with values for regional cratonic basement. Therefore, we have fixed ε_{Nd} and [Nd] values for the basaltic end member for each region (i.e. northern Laurentia, Australia, South China) in the calculations. In contrast, the cratonic basement province (CBP) end member is allowed to vary in [Nd]. The ε_{Nd} value used for the CBP end member is estimated from the compilation of ε_{Nd} data available for cratonic basement of each region (Fig. 4a, b, c).

The resulting contoured mixing lattices (Fig. 4d, e, f) can be used to calculate the contribution of CFB to the mudstone samples based on their ε_{Nd} and Nd concentrations, and hence to calculate an f_{maf} value (Figs. 4g–i, 5) for each sample. From these data, we constructed f_{maf} curves for each region by applying a 10-point locally weighted scatterplot smoothing process (LOESS). The f_{maf} profiles elucidate the prominent shift from mafic to fel-

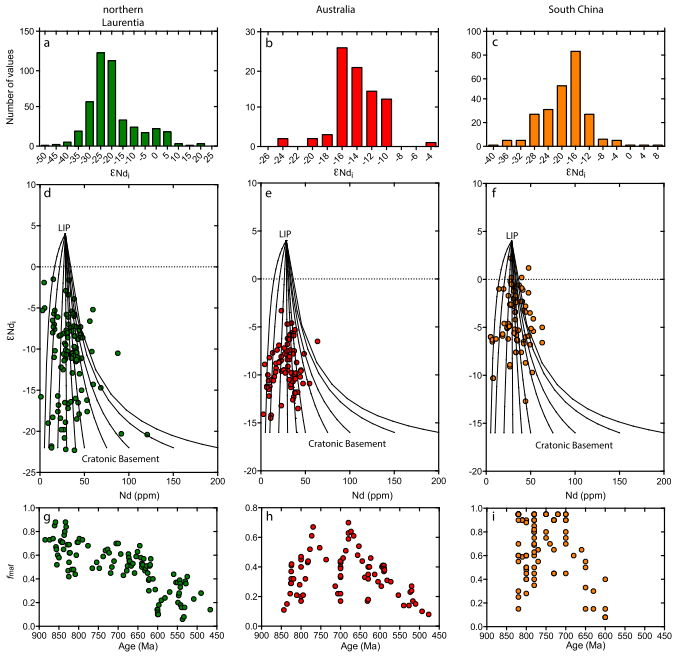

Fig. 4. Mixing model for mudstones from northern Laurentia, Australia, and South China used to calculate f_{maf} from mudstone ε_{Nd} data. (a–c) Histograms of basement ε_{Nd} compositions for northern Laurentia (NW Canada plus Svalbard), Australia, and South China. (d–f) Mixing lattices with projected mudstone data. Curved black lines are mixing lines between basalt with fixed ε_{Nd} and Nd concentration and cratonic basement with fixed ε_{Nd} but variable Nd concentration, black dots are 10% increments along the mixing line. f_{maf} was calculated by the projection of ε_{Nd} data onto the mixing lattice. All projections where done at the age of sediment deposition for each individual data point, but for simplicity are shown in summation graphically at the fixed age of 720 Ma. (g–i) Calculated f_{maf} values based on data used in compilation in Fig. 3.

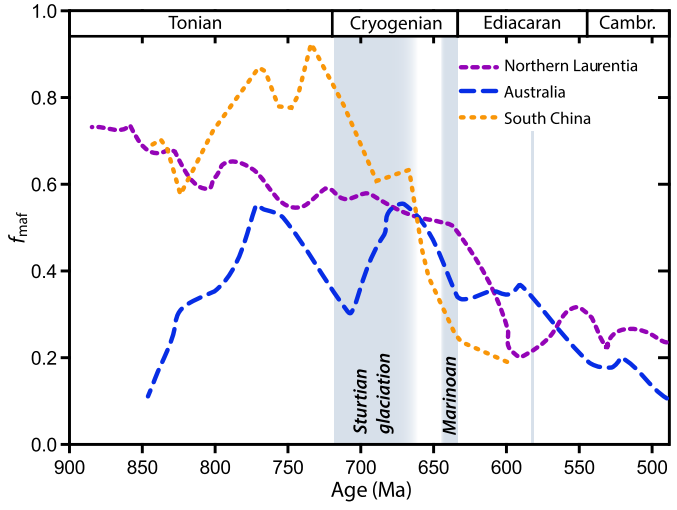

Fig. 5. Fraction (f) of detrital sediments derived from weathering of a mafic (LIP) source provenance. Mafic fractions (f_{maf}) were calculated for composite datasets from northern Laurentia (NW Laurentia plus Svalbard), Australia, and South China. Data for each region were smoothed using a ten-point LOESS fit.

sic provenance spanning the Cryogenian period (Fig. 5). During the Ediacaran, f_{maf} values from North America and Australia decline towards a dominantly CBP provenance, likely enhanced by the final stages of Rodinia break-up, which was not accompanied by massive CFB volcanism (Fig. 2b). The f_{maf} data also reveal important distinctions between regions. For example, f_{maf} rises abruptly from lower values in the early Neoproterozoic in both South China and Australia, reflecting the importance of ca. 830 Ma Willouran and Guibei LIP's in covering old continental crust with young basalts.

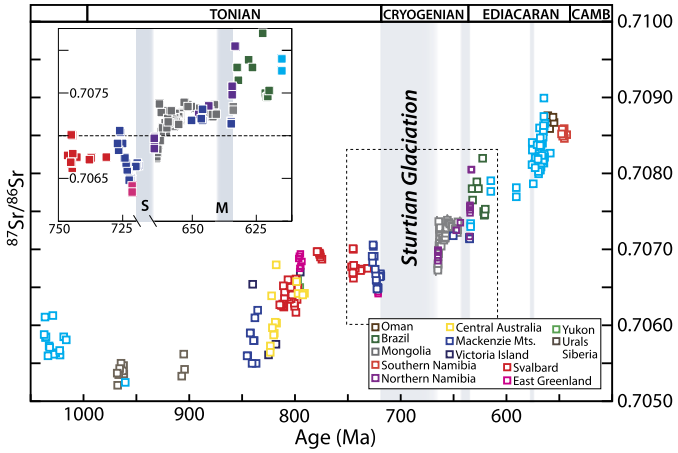

Fig. 6. Compilation of seawater $^{87}Sr/^{86}Sr$ record spanning the Neoproterozoic Era. This compilation is revised from previous versions (Halverson et al., 2007, 2010), with both new, unpublished data and previously published data. See Table S2 for a complete account of data used in this compilation. Inset shows in detail the stepwise evolution of seawater $^{87}Sr/^{86}Sr$ spanning the Cryogenian period.

In South China, the CFB contribution is >80% prior to the onset of the Cryogenian and declines to the lowest values (~0.2) by the close of the Cryogenian.

4.4. Sr isotope compilation

The compilation of $^{87}Sr/^{86}Sr$ data shown in Fig. 6 is revised from previous compilations (Halverson et al., 2007, 2010) and includes data from Kaufman et al. (1993), Burns et al. (1994), Misi and Veizer (1998), Calver (2000), Yoshioka et al. (2003) and Pokrovskii et al. (2006), with additional published data from Bartley et al. (2001), Kuznetsov et al. (2006), Melezhik et al. (2009), Rooney et al. (2014), Bold et al. (2016) and our own previously unpublished data (Table S2). For each individual succession, ages were determined, where possible, by calibration with the $\delta^{13}C_{carb}$ compilation, such that even where absolute ages are inaccurate, their relative ages should be broadly correct.

The new $^{87}Sr/^{86}Sr$ compilation (Fig. 6) reveals a pronounced trough in $^{87}Sr/^{86}Sr$ (down to 0.7053) in the early Neoproterozoic that coincides with the ca. 950–850 Ma interval between Rodinia assembly and the onset of break-up and is reminiscent of the late Paleozoic low in $^{87}Sr/^{86}Sr$ that followed the assembly of Pangaea (Burke et al., 1982). $^{87}Sr/^{86}Sr$ then rises abruptly to values >0.7060 around 850–840 Ma, prior to a decline back to ~0.7055 by 830 Ma, synchronous with the emplacement of the Willouran and Guibei LIP's. A second steep rise in $^{87}Sr/^{86}Sr$ to near 0.7070 by 800 Ma is interrupted by a shift to a roughly flat trend and a ca. 780 Ma downturn that coincides broadly with the Gunbarrel and Kanding LIP's. Following a brief recovery to values near 0.7070, $^{87}Sr/^{86}Sr$ then drops abruptly to as low as 0.7064 just prior to the onset of Cryogenian glaciation.

This pre-Cryogenian downturn is most clearly seen in data from the Coates Lake Group in the Mackenzie Mountains of NW Canada (Rooney et al., 2014), which fills small basins that were at least intermittently restricted. A similar decline is also evident in combined data from Svalbard and East Greenland. Hence, it appears that this sharp drop in $^{87}Sr/^{86}Sr$ is a true seawater signal that heralds impending snowball glaciation.

During the Cryogenian glacial interlude, $^{87}Sr/^{86}Sr$ rises abruptly to new steady state values of ~0.7073 (Fig. 6), attesting to the role of Sturtian glaciation in removing unradiogenic basalt and exposing fresh, old, continental crust (Rooney et al., 2014). Strontium isotope ratios again shift abruptly upward (to >0.7080) in the early Ediacaran, reflecting further removal of CFB cover from the conti-

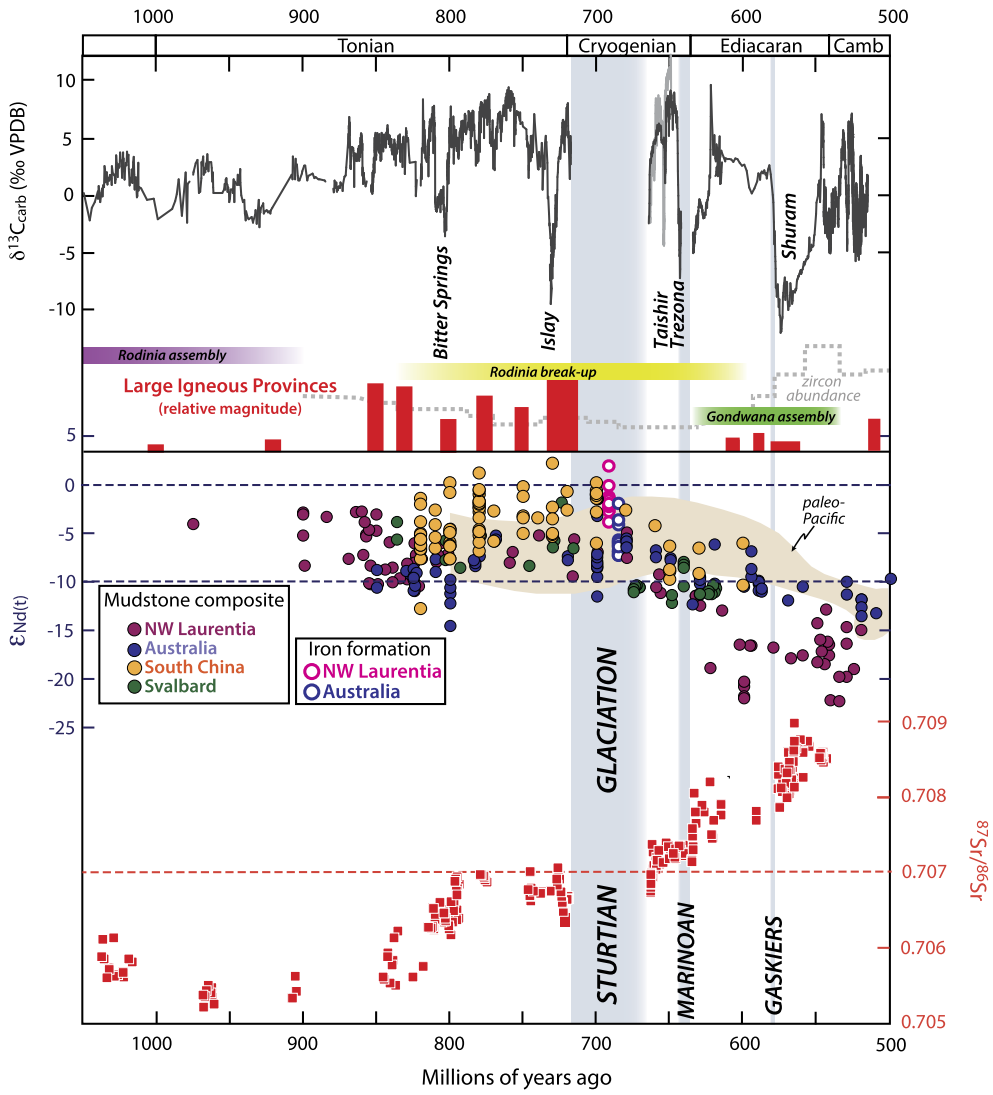

Fig. 7. Combined carbon, neodymium, and strontium isotope compilations and the LIP record for the Neoproterozoic, from Figs. 2–4. Zircon abundance is from Cawood et al. (2013). Range of Paleo-Pacific ε_{Nd} is from Keto and Jacobsen (1988).

nents and the transient effect of the silicate weathering drawdown of the extraordinarily large, post-Marinoan atmospheric CO_2 reservoir (Le Hir et al., 2009).

5. Discussion

5.1. Silicate weathering of CFB's in the Neoproterozoic

The Nd isotope compilation for mudstones and coupled f_{maf} calculations reveal an exceptionally high detrital contribution from mafic lithologies to sedimentary basins in northern Rodinian during the early–middle Neoproterozoic, followed by a sharp decline spanning the Cryogenian glaciations (Figs. 6, 7). These results are consistent with the geological record, which shows a flare-up in LIP's between ca. 850–720 Ma, with many of these clustered around northern Rodinia, followed by a lull in LIP emplacement during the latter Cryogenian and early Ediacaran periods.

Given the global paleogeography leading into Cryogenian glaciation, with the extensive CFB provinces located in the tropics (Fig. 1), it is reasonable to assume that these basalts were not only extensively physically weathered, but also intensely chemically weathered. Indeed, physical and chemical weathering are closely coupled (Gaillardet et al., 1999; Maher and Chamberlain, 2014), and several direct lines of evidence attest to the role of chemical weathering of these CFB's and their influence on riverine solute fluxes to the early Neoproterozoic oceans. First, ε_{Nd} data on marine carbonates from the paleo-Pacific Ocean (Keto and Jacobsen, 1988) show a virtually identical trend to our mudstone data (Fig. 7), with high pre-Cryogenian values and sharply declining Ediacaran values, implicating a prominent early Neoproterozoic source of dissolved juvenile Nd to seawater. Second, a compilation of chemical index of alteration (CIA) data from the studied basins in northern Rodinia shows moderately to strongly chemically weathered signatures in early Neoproterozoic samples, clearly offset from CFB and average upper continental crust (Fig. S2). Finally, the seawater strontium isotope record, which is sensitive to the abundance of CFB's due to their unradiogenic initial Sr-isotopic compositions (Taylor and Lasaga, 1999), mirrors the Nd isotope trends, providing independent evidence of the Cryogenian removal of the flood basalt carapace from northern Rodinia. Consequently the combined dataset of Nd and Sr isotopes supports enhanced silicate weathering of CFB's during the middle Neoproterozoic, and in particular leading into the Cryogenian period.

5.2. Lithological controls on phosphorus supply and the role of CFB versus arc weathering

If it is assumed that phosphorus is the limiting nutrient on geological timescales (Tyrrell, 1999), the variations in phosphorus con-

tent within continental lithologies must exert significant control on primary productivity over geological time scales. To demonstrate the importance of surficial lithology on globally integrated P fluxes from the continents, we have compiled ~14,000 analyses of Archean cratonic basement rocks, ~13,000 CFB samples, and ~68,000 arc volcanics (Fig. 8). Similar to the results of Horton (2015), these datasets reveal that the peak in P_2O_5 concentration occurs between 50–53% SiO_2, which corresponds to an overall mafic (i.e. primitive) composition. Interestingly, the broad shape of this P_2O_5 vs. SiO_2 distribution closely matches the theoretical fractional crystallization path for a basaltic melt. This suggests that the P-enrichment observed in these datasets is largely the result of the high solubility of P in basaltic magmas (Toplis et al., 1994) and that basaltic compositions are reached before apatite saturation. Adjusting this model to include the effect of assimilation and fractional crystallization (AFC) results in higher P_2O_5 for any given SiO_2 composition. Importantly, similar peak P_2O_5 concentrations also occur in basalts in arc-related volcanics (Fig. 8b), and this enrichment, as compared to oceanic equivalents (i.e. MORB; Fig. 8c) is also likely the result of AFC processes. However, whereas arc-basalts are P-enriched, most arc-related volcanics are andesitic in composition, and these contain significantly less P_2O_5 (Fig. 8b). Therefore, although arc weathering presumably plays an important role in the long-term continental P flux to the oceans, it does not have the same potential to dramatically alter P fluxes as do more rapidly emplaced and removed CFB's.

Additional evidence suggests that the variations in f_{maf} and $^{87}Sr/^{86}Sr$ spanning the Cryogenian glaciations are most likely due to weathering of CFB and not other mafic lithologies. First, with the possible exception of South China (Zhao and Zhou, 2007), volcanic arcs were absent in northern Rodinia during the middle Neoproterozoic (Li et al., 2013). And although early Neoproterozoic basins in northern Laurentia (Macdonald et al., 2012; Turner and Bekker, 2015) and Australia were the result of continental rifting prior to the onset of Rodinia break-up, these rifting events were largely non-magmatic. Nor did fluctuations in arc length likely contribute significantly to a global increase in mafic weathering in the middle Neoproterozoic. Both theoretical considerations (Silver and Behn, 2008) and global U–Pb zircon age compilations (Cawood et al., 2013; McKenzie et al., 2014; Roberts and Spencer, 2015) (Fig. 7) suggest that total continental arc length was near a long-term minimum leading into Cryogenian glaciation and did not peak until the late Ediacaran—coincident with the Neoproterozoic maximum in $^{87}Sr/^{86}Sr$. Consequently, although we cannot rule out a contribution of juvenile Nd from isolated rift- or arc-related volcanics, we interpret the f_{maf} values (Fig. 6) to reflect principally the contribution of CFB weathering relative to the underlying continental basement.

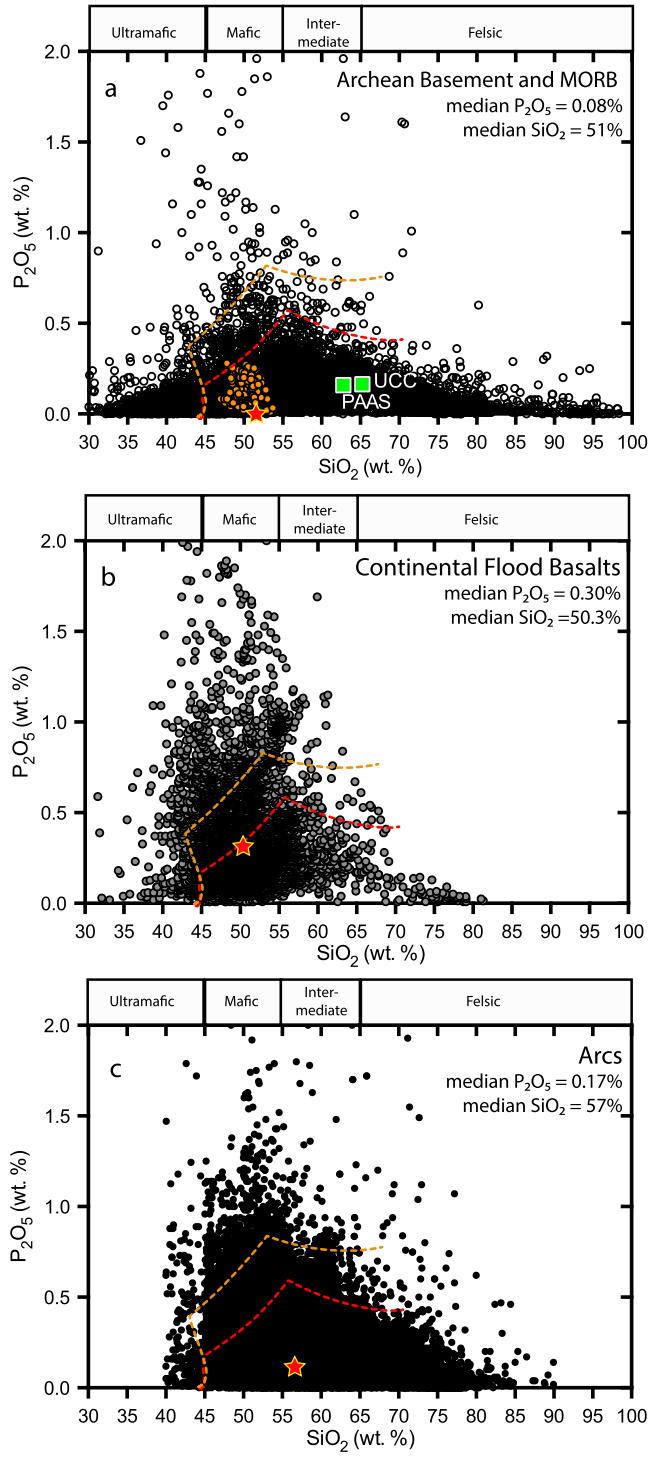

Fig. 8. Phosphorus in igneous rocks. (a) A compilation of ~14,000 analyses of Archean basement rocks (open circles) reveals that peak P_2O_5 concentration occurs between 50 and 53% SiO_2 corresponding to broadly basaltic compositions. The average composition of the Upper Continental Crust (UCC) and Post Archean Australian Shale (PAAS) have compositions that lie far to the right of the P_2O_5 peak. Orange circles are a compilation of ~600 mid ocean ridge basalt (MORB) samples that have P_2O_5 concentrations similar to the UCC and PAAS. (b) A compilation of ~13,000 Continental Flood Basalt (CFB) samples which share a similar P_2O_5 trend with respect to SiO_2 as Archean basement rocks. Whereas peak P_2O_5 for CFB also occurs at broadly basaltic compositions, it is evident that CFB's have even higher P_2O_5 concentrations than Archean basement (median P_2O_5 of CFB is 3.75 times great than that of Archean basement) making them a significant source of P_2O_5. Values for UCC and PAAS are from Taylor and McLennan (1985, 1995). (c) A compilation of ~68,000 convergent margin (i.e. arc) volcanic samples again showing that peak P_2O_5 concentrations are associated with basaltic compositions. Median P_2O_5 for this arc compilation is 0.17%. In all diagrams, the red dashed line is the theoretical fractional crystallization (FC) path for a primitive basaltic melt, which reveals the high solubility of P in melts of basaltic composition and that such compositions are reached before apatite saturation (apatite saturation occurs at the major downward deflection in the red and orange dashed lines). Consequently, P is not depleted by removal associated with a fractionating P bearing phase. Furthermore, when erupted, P will be concentrated in easily weathered volcanic glass and not in highly resistant apatite. Orange line is the assimilation and fractional crystalization (AFC) path where the assimilating material is the upper continental crust. Red stars show the medium SiO_2 and P_2O_5 for each compilation. FC and AFC paths were calculated using the alphaMELTS modeling software (Ghiorso and Sack, 1995; Smith and Asimow, 2005). Archean basement, CFB and arc data is from the GEOROC repository (http://georoc.mpch-mainz.gwdg.de/georoc/Start.asp) while MORB data is from Jenner and O'Neill (2012). (For interpretation of the references to color in this figure legend, the reader is referred to the web version of this article.)

5.3. The biogeochemical impact of CFB weathering

Previous estimates by Horton (2015) and a compilation of chemical index of alteration (CIA) data from the studied basins (Fig. S1) indicate that approximately half of the initial mass of CFB source rocks was dissolved via chemical weathering during the Neoproterozoic. Given that CFB's have on average ~3 times as much P as typical continental crust, with much of this P residing in the fine-grained matrix (i.e., glass), and that Neoproterozoic LIP's, in particular the ca. 780 Ma Gunbarrel LIP (median $P_2O_2 \approx 0.5$), are exceptionally rich in P (Horton, 2015), it follows that the early–middle Neoproterozoic would have experienced a sustained, anomalously high continental flux of phosphorus to the global oceans. This P flux was likely coupled to iron via adsorption onto ferric oxyhydroxides formed during oxidative weathering (Laakso and Schrag, 2014) of the CFB's and subsequent liberation in estuaries by desorption upon mixing of river and seawater (Froelich, 1988) and in porewaters of anoxic continental margin sediments by a combination of dissimilatory iron reduction, which likely played an important role in Precambrian iron cycling (Severmann et al., 2008; Li et al., 2015), and sulfide-catalyzed reduction of iron oxides (Poulton et al., 2015).

Direct evidence for the elevated terrestrial P flux in the Neoproterozoic is seen in the marked phosphorus enrichment observed in Cryogenian iron formation (Planavsky et al., 2010), which is thought to be the result of leaching of continental margin sediments dominated by basaltic detritus (Cox et al., 2016). Indirect evidence of the elevated P flux is found in the exceptionally high $\delta^{13}C_{carb}$ values that prevailed through much of the early–middle Neoproterozoic. Assuming that P limited net primary productivity, then it follows that increased P would have increased organic carbon burial. Because the increased P flux would typically be accompanied by increased alkalinity flux (hence higher inorganic carbon burial) (Holland, 1984; Holland and Bekker, 2012), this factor alone should not strongly influence $\delta^{13}C_{carb}$. However, our calculations show that $P/(CO_2D)$ ratios — a measure of the P released compared to CO_2 consumed during dissolution, and ultimately alkalinity generated by this process, is ~3 times greater for average CFB than for either average continental basement or mid-ocean ridge basalt (see supplementary information). Therefore, higher organic carbon burial would also have translated into higher fractional organic carbon burial (f_{org} = organic carbon burial/total carbon burial) and higher $\delta^{13}C_{carb}$ values, consistent with typically ^{13}C-enriched carbonates during the early–middle Neoproterozoic (up to +8‰; Fig. 7). Conversely, the decrease in f_{maf} from ~0.6 to ~0.3 across the Cryogenian implies a six-fold decrease in total P flux from northern Rodinia, and this decline aligns with the observation that average $\delta^{13}C_{carb}$ values are much lower in the Ediacaran than in the early Neoproterozoic (Fig. 2).

Importantly, although it is likely that fertilization via weathering of CFB's helps to explain early–middle Neoproterozoic carbon isotope record (Horton, 2015), this mechanism alone cannot explain the very high average $\delta^{13}C_{carb}$ that prevailed for most of this time. Based on a simple model of the exogenic carbon cycle in which f_{org} is controlled by the P flux (see supplementary information), we find that the increased P flux from CFB weathering accounts for ~ 2‰ of the $\delta^{13}C_{carb}$ values above the typical Proterozoic background of 0‰. Consequently, other factors are required to explain the sustained high $\delta^{13}C_{carb}$. One explanation for further enhancement in organic carbon burial is the redox-dependent P-feedback (Van Cappellen and Ingall, 1994), by which organic-bound P would have been efficiently recycled during anaerobic remineralization of primary organic matter under the dominantly anoxic deep waters (Sperling et al., 2013) of the early Neoproterozoic oceans. Another factor contributing to the high $\delta^{13}C_{carb}$ values may have been authigenic carbonate production and burial (Schrag et al., 2013), which would have been enhanced on continental shelves experiencing high primary production (Higgins et al., 2009).

5.4. A CFB-weathering trigger for snowball glaciation?

At the onset of the Cryogenian period, the Franklin CFB sat entirely within the tropics (Denyzsyn et al., 2009a, 2009b) (Fig. 1) where it would have had maximal impact on atmospheric CO_2 due to the sensitivity of hydrolysis reactions to temperature and rainfall (Dessert et al., 2003; Allègre et al., 2010; Kent and Muttoni, 2013). Seawater proxies from NW Laurentia are consistent with intense weathering of the Franklin LIP leading into the Sturtian Snowball glaciation: $^{87}Sr/^{86}Sr$ declined sharply from 0.7071 to 07064 (Fig. 2e) and $^{187}Os/^{188}Os$ fell synchronously with a rapid return to highly positive $\delta^{13}C_{carb}$ values following the ca. 735–730 Ma Islay excursion (Rooney et al., 2014). This drop in $^{87}Sr/^{86}Sr$ dwarfs similar declines following emplacement of large Phanerozoic LIP's (Fig. S6), including CAMP, for which an abrupt decline in atmospheric CO_2 has been reported (Schaller et al., 2012). Hence, chemical weathering in the pre-Cryogenian (i.e., Tonian) interval was exceptionally dominated by the hydrolysis of CFB's in the tropics.

In addition to the increase basalt weathering at this time, the accompanying elevated P flux fueled greater primary productivity, raising f_{org} (as seen in the sharp rise in $\delta^{13}C_{carb}$ following the Islay negative anomaly), expanding anoxia on proximal continental margins, and increasing biological drawdown of atmospheric CO_2. This eutrophication would have both increased P recycling—providing a strong positive feedback to primary productivity—and transiently drawn down CO_2 due to increased alkalinity generated by bacterial iron and sulfate reduction (Tziperman et al., 2011). Under prevailing conditions of already low atmospheric CO_2 levels due to enhanced silicate weathering, this alkalinity pump to the deep ocean may have provided the final nudge past the critical pCO_2 threshold (Hoffman et al., 1998; Goddéris et al., 2003; Donnadieu et al., 2004) for triggering runaway glaciation.

6. Conclusions

Coupled Nd and Sr isotope data sets for the Neoproterozoic reveal that weathering of unusually extensive continental flood basalts between ca. 850 and 717 Ma dominated the global silicate weathering feedback and continental chemical fluxes to the oceans. This effect was enhanced in the middle Neoproterozoic as the Rodinia supercontinent drifted into the tropics and began to rift apart, exposing more of these CFB's to warm, moist conditions that increased the rates of hydrolysis reactions. These CFB's were largely (but not exclusively) clustered in northern Laurentia and neighboring cratons (Fig. 1). Because CFB's are strongly enriched in phosphorus relative to typical continental crust, the high weathering rate of the CFB's would have fertilized the global oceans (Horton, 2015). High riverine P fluxes, combined with extensive anoxia on continental margins (Sperling et al., 2013), would have promoted efficient P recycling, sustaining high rates of organic carbon burial, as indicated by the carbon isotope record at this time. This additional control of CFB weathering on atmospheric CO_2 levels adds credibility to the Fire and Ice hypothesis (Goddéris et al., 2003; Donnadieu et al., 2004), in which it is argued that weathering of CFB's lowered pCO_2 sufficiently to trigger snowball glaciation. Our new data suggest specifically that it was the emplacement and rapid weathering of the Franklin LIP that pushed the Earth system across this critical threshold and ushered in the extraordinary climatic and geochemical perturbations that characterize the Neoproterozoic Era.

If intensified chemical weathering of Neoproterozoic CFB's and coupled fertilization of the oceans (Horton, 2015) triggered glaciation through rapid consumption of CO_2, Snowball glaciation itself was a powerful negative feedback on CFB weathering. It was previously argued that Cryogenian glaciation would have radically altered the global continental surface by removing a veneer of infertile regolith that developed on continental interiors and leaving behind a fresh, weatherable surface (Swanson-Hysell et al., 2010). Perhaps more importantly, Cryogenian glaciations stripped the continents of their blanket of basalt, removing the source of nutrients that sustained long-lived positive carbon isotope perturbation and preventing subsequent snowball glaciations.

Acknowledgements

This research was partially supported by Natural Sciences and Engineering Research Council of Canada (NSERC) Discovery grants to GPH and RSS, an NSERC Vanier fellowship to GMC, the Yukon Geological Survey, Polar Continental Shelf Program, and an NSF graduate research fellowship to JVS. GPH acknowledges donors of the American Chemical Society Petroleum Research Fund for partial support of this research. FAM acknowledges NSF Sedimentary Geology and Paleontology and the NASA Astrobiology Institute for support. This manuscript benefited from reviews by Andrey Bekker and 2 anonymous reviewers. Lee Kump and John Hayes provided valuable feedback on earlier drafts of this manuscript.

Appendix A. Supplementary material

Supplementary material related to this article can be found online at http://dx.doi.org/10.1016/j.epsl.2016.04.016.

References

Allègre, C.J., Louvat, P., Gaillardet, J., Meynadier, L., Rad, S., Capmas, F., 2010. The fundamental role of island arc weathering in the oceanic Sr isotope budget. Earth Planet. Sci. Lett. 292, 46–51.

Ariskin, A.A., Kostitsyn, Y.A., Konnikov, E.G., Danyushevsky, L.V., Meffre, S., Nikolaev, G.S., McNeill, A., Kislov, E.V., Orsoev, D.A., 2013. Geochronology of the Dovyren intrusive complex, Northwestern Baikal area, Russia, in the Neoproterozoic. Geochem. Int. 51, 859–875.

Bahlburg, H., Dobrzinksi, N., 2011. A review of the Chemical Index of Alteration (CIA) and its application to the study of Neoproterozoic glacial deposits and climate transitions. In: Arnaud, E., Halverson, G.P., Shields-Zhou, G. (Eds.), The Geological Record of Neoproterozoic Glaciations. In: Mem. Geol. Soc. Lond., vol. 36, pp. 81–92.

Barovich, K.M., Foden, J., 2000. A Neoproterozoic flood basalt province in southern-central Australia: geochemical and Nd isotope evidence from basin fill. Precambrian Res. 100, 213–234.

Bartley, J.K., Semikhatov, M.A., Kaufman, A.J., Knoll, A.H., Pope, M.C., Jacobsen, S.B., 2001. Global events across the Mesoproterozoic–Neoproterozoic boundary: C and Sr isotopic evidence from Siberia. Precambrian Res. 111, 165–202.

Blackburn, T.J., et al., 2013. Zircon U–Pb geochronology links the End-Triassic mass extinction with the Central Atlantic Magmatic Province. Science 340, 941–945.

Bold, U., Smith, E.F., Rooney, A.D., Bowring, S.A., Buchwaldt, R., Dúdas, F.Ö., Ramezani, J., Crowley, J.L., Schrag, D.P., Macdonald, F.M., 2016. Neoproterozoic stratigraphy of the Zavkhan Terrane of Mongolia: the backbone for Cryogenian and early Ediacaran chemostratigraphic records. Am. J. Sci. 316, 1–63.

Burke, W.H., Denison, R.E., Hetherington, E.A., Koepnick, R.B., Nelson, H.F., Otto, J.B., 1982. Variation of seawater $^{87}Sr/^{86}Sr$ through Phanerozoic time. Geology 10, 516–519.

Burns, S.J., Haudenschild, U., Matter, A., 1994. The strontium isotopic composition of carbonates from the Late Precambrian (~560–540 Ma) Huqf Group of Oman. Chem. Geol. 111, 269–282.

Calver, C., 2000. Isotope stratigraphy of the Ediacaran (Neoproterozoic III) of the Adelaide rift complex, Australia, and the overprint of water column stratification. Precambrian Res. 100, 121–150.

Cawood, P.A., Hawkesworth, C.J., Dhuime, B., 2013. The continental record and the generation of continental crust. Geol. Soc. Am. Bull. 125, 14–32.

Colpron, M., Logan, J.M., Mortensen, J.K., 2003. U–Pb zircon age constraint for late Neoproterozoic rifting and initiation of the lower Paleozoic passive margin of western Laurentia. Can. J. Earth Sci. 39, 133–143.

Condon, D., Zhu, M., Bowring, S.A., Jin, Y., Yang, A., 2005. From the Marinoan glaciation to the oldest bilaterians: U–Pb ages from the Doushantuo Formation, China. Science 308, 95–98.

Courtillot, V., Jaupart, C., Manighetti, I., Tapponier, P., Besse, J., 1999. On causal links between flood basalts and continental breakup. Earth Planet. Sci. Lett. 166, 177–195.

Cox, G.M., Halverson, G.P., Poirier, A., Le Heron, D., Strauss, J.V., Stevenson, R., 2016. A model for Cryogenian iron formation. Earth Planet. Sci. Lett. 433, 280–292.

Cox, G.M., Strauss, J.V., Halverson, G.P., Schmitz, M.D., McClelland, W.C., Stevenson, R.S., Macdonald, F.A., 2015. Kikiktat volcanics of Arctic Alaska—melting of harzburgitic mantle associated with the Franklin large igneous province. Lithosphere 7, 275–295.

Denyszyn, S.W., Halls, H.C., Davis, D.W., Evans, D.A.D., 2009a. Paleomagnetism and U–Pb geochronology of Franklin dykes in High Arctic Canada and Greenland: a revised age and paleomagnetic pole constraining block rotations in the Nares Strait region. Can. J. Earth Sci. 46, 689–705.

Denyszyn, S.W., Davis, D.W., Hall, H.C., 2009b. Paleomagnetism and U–Pb geochronology of the Clarence Head dykes, Arctic Canada: orthogonal emplacement of mafic dykes in a large igneous province. Can. J. Earth Sci. 46, 155–167.

Dessert, C., Dupré, B., Gaillardet, J., François, L.M., Allègre, C.J., 2003. Basalt weathering laws and the impact of basalt weathering on the global carbon cycle. Chem. Geol. 202, 257–273.

Dessert, C., et al., 2001. Erosion of Deccan Traps determined by river geochemistry: impact on the global climate and the $^{87}Sr/^{86}Sr$ ratio of seawater. Earth Planet. Sci. Lett. 188, 459–474.

Donnadieu, Y., Goddéris, Y., Ramstein, G., Nédélec, A., Meert, J., 2004. A snowball Earth climate triggered by continental break-up through changes in runoff. Nature 428, 303–306.

Edwards, C.T., Saltzman, M.R., Leslie, S.A., Bergström, S.M., Sedlacek, A.R.C., Howard, A., Bauer, J.A., Sweet, W.C., Young, S.A., 2015. Strontium isotope ($^{87}Sr/^{86}Sr$) stratigraphy of Ordovician bulk carbonate: implications for preservation of primary values. Geol. Soc. Am. Bull. 127, 1275–1289.

Ernst, R.E., Bleeker, W., Söderland, U., Kerr, A.C., 2013. Large Igneous Provinces and supercontinents: towards the complete tectonic revolution. Lithos 174, 1–14.

Ernst, R.E., Wingate, M.T.D., Buchan, K.L., Li, Z.-X., 2008. Global record of 1600–700 Ma Large Igneous Provinces (LIPs): implications for the reconstruction of the proposed Nuna (Columbia) and Rodinia supercontinents. Precambrian Res. 160, 159–178.

Fike, D.A., Grotzinger, J.P., Pratt, L.M., Summons, R.E., 2006. Oxidation of the Ediacaran Ocean. Nature 44, 744–747.

Froelich, P.N., 1988. Kinetic control of dissolved phosphate in natural rivers and estuaries: a primer on the phosphate buffer mechanism. Limnol. Oceanogr. 33, 649–668.

Gaillardet, J., Dupré Louvat, P., Allègre, C., 1999. Global silicate weathering and CO_2 consumption rates deduced from the chemistry of large rivers. Chem. Geol. 159, 3–30.

Ghiorso, M.S., Sack, R.O., 1995. Chemical mass transfer in magmatic processes IV. A revised and internally consistent thermodynamic model for the interpolation and extrapolation of liquid–solid equilibria in magmatic systems at elevated temperatures and pressures. Contrib. Mineral. Petrol. 119, 197–212.

Goddéris, Y., Donnadieu, Y., Nédélec, A., Dupré, B., Dessert, C., Grard, A., Ramstein, G., François, L., 2003. The Sturtian 'snowball' glaciation: fire and ice. Earth Planet. Sci. Lett. 211, 1–12.

Halverson, G., 2006. A Neoproterozoic chronology. In: Neoproterozoic Geobiology and Paleobiology, pp. 231–271.

Halverson, G.P., Dudás, F.Ö., Maloof, A.C., Bowring, S.A., 2007. Evolution of the $^{87}Sr/^{86}Sr$ composition of Neoproterozoic seawater. Palaeogeogr. Palaeoclimatol. Palaeoecol. 256, 103–129.

Halverson, G.P., Hoffman, P.F., Schrag, D.P., Kaufman, A.J., 2002. A major perturbation of the carbon cycle before the Ghaub glaciation (Neoproterozoic) in Namibia: prelude to snowball Earth? Geochem. Geophys. Geosyst. 3, 1–24. http://dx.doi.org/10.1029/2001GC000244.

Halverson, G.P., Hoffman, P.F., Schrag, D.P., Maloof, A.C., Rice, A.H., 2005. Toward a Neoproterozoic composite carbon-isotope record. Geol. Soc. Am. Bull. 117, 1181–1207.

Halverson, G.P., Wade, B.P., Hurtgen, M.T., Barovich, K., 2010. Neoproterozoic chemostratigraphy. Precambrian Res. 182, 337–350.

Heaman, L.H., LeCheminant, A.N., Rainbird, R.H., 1992. Nature and timing of Franklin igneous events, Canada: implications for a Late Proterozoic mantle plume and the break-up of Laurentia. Earth Planet. Sci. Lett. 109, 117–131.

Higgins, J.A., Schrag, D.P., Fischer, W.W., 2009. Oxygenation of the oceans and sediments: consequences for the seafloor carbonate factory. Earth Planet. Sci. Lett. 284, 25–33.

Hill, A.C., Haines, P.W., Grey, K., 2011. Neoproterozoic glacial deposits of central Australia. In: Arnaud, E., Halverson, G.P., Shields-Zhou, G. (Eds.), The Geological Record of Neoproterozoic Glaciations. In: Mem. Geol. Soc. Lond., vol. 36, pp. 677–691.

Hoffman, P.F., Kaufman, A.J., Halverson, G.P., Schrag, D.P., 1998. A neoproterozoic Snowball Earth. Science 281, 1342–1346.

Holland, H., 1984. The Chemical Evolution of the Oceans and Atmosphere. Princeton University Press.

Horton, F., 2015. Did phosphorus derived from the weathering of large igneous provinces fertilize the Neoproterozoic ocean? Geochem. Geophys. Geosyst. 16, 1723–1738.
Jenner, F.E., O'Neill, H.S.C., 2012. Analysis of 60 elements in 616 ocean floor basaltic glasses. Geochem. Geophys. Geosyst. 13, Q02005.
Johnston, D., Poulton, S.W., Tosca, N., O'Brien, T., Halverson, G.P., Schrag, D.P., Macdonald, F.A., 2013. Searching for an oxygenation event in the fossiliferous Ediacaran of northwestern. Canada. Chem. Geol. 362, 273–286.
Kaufman, A.J., Jacobsen, S.B., Knoll, A.H., 1993. The Vendian record of Sr and C isotopic variations in seawater: implications for tectonics and paleoclimate. Earth Planet. Sci. Lett. 120, 409–430.
Kent, D.V., Muttoni, G., 2013. Modulation of Late Cretaceous and Cenozoic climate by variable drawdown of atmospheric pCO_2 provinces on continents drifting through the equatorial humid belt. Clim. Past 9, 525–546.
Keto, L.S., Jacobsen, S.B., 1988. Nd isotopic variation of Phanerozoic paleooceans. Earth Planet. Sci. Lett. 90, 395–410.
Klein, C., Beukes, N.J., 1993. Sedimentology and geochemistry of the glaciogenic Late Proterozoic Rapitan iron-formation in Canada. Econ. Geol. 88, 542–565.
Knoll, A.H., Kaufman, A.J., Semikhatov, M.A., 1995. The carbon-isotopic composition of Proterozoic carbonates; Riphean successions from northwestern Siberia (Anabar Massif, Turukhansk Uplift). Am. J. Sci. 295, 823–850.
Kunzmann, M., Halverson, G.P., Scott, C.T., Minarik, W.G., Wing, B.A., 2015. Geochemistry of Neoproterozoic black shales from Svalbard: implications for ocean redox conditions spanning Cryogenian glaciations. Chem. Geol. 417, 383–393.
Kuznetsov, A.B., Semikhatov, M.A., Maslov, A.V., Gorokhov, I.M., Prasolov, E.M., Krupenin, M.T., Kislova, I.V., 2006. New data on Sr- and C-isotopic chemostratigraphy of the Upper Riphean type section (Southern Urals). Stratigr. Geol. Correl. 14, 602–628.
Laakso, T.A., Schrag, D.P., 2014. Regulations of atmospheric oxygen during the Proterozoic. Earth Planet. Sci. Lett. 388, 81–91.
Le Guerroué, E., Allen, P.A., Cozzi, A., 2006. Chemostratigraphic and sedimentological framework of the largest negative carbon isotopic excursion in Earth history: the Neoproterozoic Shuram Formation, Nafun Group, Oman. Precambrian Res. 146, 68–92.
Le Hir, G., Donnadieu, Y., Goddéris, Y., Pierrehumbert, R.T., Halverson, G.P., Macouin, M., Nédélec, A., Ramstein, G., 2009. The snowball Earth aftermath: exploring the limits of continental weathering processes. Earth Planet. Sci. Lett. 277, 453–463.
Lefebvre, V., Donnadieu, Y., Goddéris, Y., Fluteau, F., Hubert-Théou, L., 2013. Was the Antarctic glaciation delayed by a high degassing rate during the early Cenozoic? Earth Planet. Sci. Lett. 371–372, 203–211.
Li, W., Beard, B.L., Johnson, C., 2015. Biologically recycled continental iron is a major component in banded iron formations. Proc. Natl. Acad. Sci. USA 112, 8193–8198.
Li, Z.-X., Evans, D.A.D., Halverson, G.P., 2013. Neoproterozoic glaciations in a revised global paleogeography. Sediment. Geol. 294, 219–232.
Macdonald, F.A., Jones, D.S., Schrag, D.P., 2009. Stratigraphic and tectonic implications of a newly discovered glacial diamictite–cap carbonate couplet in southwestern Mongolia. Geology 37, 123–126.
Macdonald, F.A., Schmitz, M.D., Crowley, J.L., Roots, C.F., Jones, D.S., Maloof, A.C., Strauss, J.V., Cohen, P.A., Johnston, D.T., Schrag, D.P., 2010. Calibrating the Cryogenian. Science 327, 1241–1243.
Macdonald, F.M., Halverson, G.P., Strauss, J.V., Smith, E.F., Cox, C.M., Sperling, E., Roots, C.F., Schrag, D.P., 2012. Early Neoproterozoic basin formation in the Yukon: implications for the make-up and break-up of Rodinia. Geosci. Can. 39, 77–97.
Maher, K., Chamberlain, C.P., 2014. Hydrologic regulation of chemical weathering and the geologic carbon cycle. Science 343, 1502–1504.
Maloof, A.C., Porter, S.M., Moore, J.L., Dudás, F.Ö., Bowring, S.A., Higgins, J.A., Fike, D.A., Eddy, M.P., 2010. The earliest Cambrian record of animals and ocean geochemical change. Geol. Soc. Am. Bull. 122, 1731–1774.
McArthur, J., Howarth, R.J., 2012. Strontium isotope stratigraphy. In: Shields, G.A. (Ed.), The Geological Time Scale. Elsevier, pp. 127–144. Ch. 7.
McCausland, P.J.A., Hankard, F., Van der Voo, R., Hall, C.M., 2011. Ediacaran paleogeography of Laurentia: paleomagnetism and geochronology of the 583 Ma Bae de Moutons syenite, Quebec. Precambrian Res. 187, 58–78.
McKenzie, N.R., Hughes, N.C., Gill, B.C., Myrow, P.M., 2014. Plate tectonic influences on Neoproterozoic–early Paleozoic climate and animal evolution. Geology 42, 127–130.
Melezhik, V.A., Pokrovsky, B.G., Fallick, A.E., Kuznetsov, A.B., Bujakaite, M.I., 2009. Constraints on the $^{87}Sr/^{86}Sr$ of Late Ediacaran seawater: insights from high-Sr limestones. J. Geol. Soc. (Lond.) 166, 183–191.
Mills, B., Daines, S.J., Lenton, T.M., 2014. Changing tectonic controls on the long-term climate cycle from Mesozoic to present. Geochem. Geophys. Geosyst. 15, 4866–4884.
Misi, A., Veizer, J., 1998. Neoproterozoic carbonate sequences of the Una Group, Irece Basin, Brazil: chemostratigraphy, age and correlations. Precambrian Res. 89, 87–100.
Nabelek, P.I., Bédard, J.H., Rainbird, R.H., 2014. Numerical constraints on degassing of metamorphic CO_2 during the Neoproterozoic large igneous event, Arctic Canada. Geol. Soc. Am. Bull. 126, 759–772.
Planavsky, N.J., Rouxel, O.J., Bekker, A., Lalonde, S.V., Konhauser, K.O., Reinhard, C.T., Lyons, T.W., 2010. The evolution of the marine phosphate reservoir. Nature 467, 1088–1090.
Pokrovskii, B.G., Melezhik, V.A., Bujakaite, M.I., 2006. Carbon, oxygen, strontium, and sulfur isotopic compositions in late Precambrian rocks of the Patom Complex, central Siberia: communication 1. Results, isotope stratigraphy, and dating problems. Lithol. Miner. Resour. 41, 450–474.
Poulton, S.W., Henkel, S., März, C., Urquhart, H., Flögel, S., Kasten, S., Sinninghe Damsté, J.S., Wagner, T., 2015. A continental-weathering control on orbitally driven redox-nutrient cycling during Cretaceous Ocean Anoic Event 2. Geology 43, 963–966.
Rainbird, R.H., Jefferson, C.W., Young, G.M., 1996. The early Neoproterozoic sedimentary Succession B of northwestern Laurentia: correlations and paleogeographic significance. Geol. Soc. Am. Bull. 108, 454–470.
Ravizza, G., Peucker-Ehrenbrink, B., 2003. Chemostratigraphic evidence of Deccan volcanism from the marine osmium isotope record. Science 302, 1392–1395.
Roberts, N.M.W., Spencer, C.J., 2015. The zircon archive of continent formation through time. Geol. Soc. (Lond.) Spec. Publ. 389, 197–225.
Rooney, A.D., Macdonald, F.A., Strauss, J.V., Dudás, F.Ö., Hallmann, C., Selby, D., 2014. Re–Os geochronology and coupled Os–Sr isotope constraints on the Sturtian snowball Earth. Proc. Natl. Acad. Sci. USA 111, 51–56.
Rooney, A.D., Strauss, J.V., Brandon, A.D., Macdonald, F.A., 2015. A Cryogenian chronology: two long-lasting synchronous Neoproterozoic glaciations. Geology 43, 459–462.
Schaller, M.F., Wright, J.D., Kent, D.V., 2011. Atmospheric PCO_2 perturbations associated with the Central Atlantic Magmatic Province. Science 331, 1404–1408.
Schaller, M.F., Wright, J.D., Kent, D.V., Olsen, P.E., 2012. Rapid emplacement of the Central Atlantic Magmatic Province as a net sink for CO_2. Earth Planet. Sci. Lett. 323–324, 27–39.
Schrag, D.P., Berner, R.A., Hoffman, P.F., Halverson, G.P., 2002. On the initiation of snowball Earth. Geochem. Geophys. Geosyst. 3. http://dx.doi.org/10.1029/2001GC000219.
Schrag, D.P., Higgins, J.A., Macdonald, F.A., Johnston, D.T., 2013. Authigenic carbonate and the history of the global carbon cycle. Science 339, 540–543.
Severmann, S., Lyons, T.W., Anbar, A., McManus, J., Gordon, G., 2008. Modern iron isotope perspective on the benthic iron shuttle and the redox evolution of ancient oceans. Geology 36, 487–490.
Silver, P.G., Behn, M.G., 2008. Intermittent plate tectonics? Science 319, 18–85.
Smith, P.M., Asimow, P.D., 2005. Adiabat_1ph: a new public front-end to the MELTS, pMELTS, and pHMELTS models. Geochem. Geophys. Geosyst. 6, 1–8.
Sobolev, A.V., Hofmann, A.W., Kuzmin, D.V., Yaxley, G.M., Arndt, N.T., Chung, S.-L., Danyushevsky, L.V., Elliott, T., Frey, F.A., Garcia, M.O., Gurenko, A.A., Kamenetsky, V.S., Kerr, A.C., Krivolutskaya, N.A., Matvienkov, V.V., Nikogosian, I.K., Rocholl, A., Sigurdsson, I.A., Sushchevskaya, N.M., Teklay, M., 2007. The amount of recycled crust in sources of mantle-derived melts. Science 316, 412–417.
Sobolev, S.V., Sobolev, A.V., Kuzmin, D.V., Krivolutskaya, N.A., Petrunin, A.G., Arndt, N.T., Radko, V.A., Vasiliev, Y.R., 2011. Linking mantle plumes, large igneous provinces and environmental catastrophes. Nature 477, 312–316.
Sperling, E.A., Halverson, G.P., Knoll, A.H., Macdonald, F.A., Johnston, D.T., 2013. A basin redox transect at the dawn of animal life. Earth Planet. Sci. Lett. 371–372, 143–155.
Strauss, J.V., Rooney, A.D., Macdonald, F.A., Brandon, A.D., Knoll, A.H., 2014. 740 Ma vase-shaped microfossils from Yukon, Canada: implications for Neoproterozoic geochronology and biostratigraphy. Geology 42, 659–662.
Swanson-Hysell, N.L., Rose, C.V., Calmet, C.C., Halverson, G.P., Hurtgen, M.T., Maloof, A.C., 2010. Cryogenian glaciation and the onset of carbon-isotope decoupling. Science 328, 608–611.
Taylor, A.S., Lasaga, A.C., 1999. The role of basalt weathering in the Sr isotope budget of the oceans. Chem. Geol. 161, 199–214.
Taylor, S.R., McLennan, S.M., 1985. The Continental Crust: Its Composition and Evolution. Blackwell, Oxford. 312 pp.
Taylor, S.R., McLennan, S.M., 1995. The geochemical evolution of the continental crust. Rev. Geophys. 33, 241–265.
Toplis, M.J., Libourel, G., Carroll, M.R., 1994. The role of phosphorus in crystallisation processes of basalt: an experimental study. Geochim. Cosmochim. Acta 58, 797–810.
Turner, E.C., Bekker, A., 2015. Thick sulfate evaporite accumulations marking a mid-Neoproterozoic oxygenation event (Ten Stone Formation, Northwest Territories, Canada). Geol. Soc. Am. Bull. 128, 203–222.
Tyrrell, T., 1999. The relative influences of nitrogen and phosphorus on oceanic primary production. Nature 400, 525–531.
Tziperman, E., Halevy, I., Johnston, D.T., Knoll, A.H., Schrag, D.P., 2011. Biologically induced initiation of Neoproterozoic snowball-Earth events. Proc. Natl. Acad. Sci. USA 108, 15091–15096.
Van Cappellen, P., Ingall, E.D., 1994. Benthic phosphorus regeneration, net primary production, and ocean anoxia: a model of the coupled marine biogeochemical cycles of carbon and phosphorus. Paleoceanography 9, 677–692.
Wade, B.P., Hand, M., Barovich, K.M., 2005. Nd isotopic and geochemical constraints on provenance of sedimentary rocks in the eastern Officer Basin, Australia: implications for the intracratonic Petermann Orogeny. Geol. Soc. 162, 513–530.

Wang, X.-C., Li, Z.-X., Li, X.-H., Li, W.-L., Zhang, Q.-R., 2011. Geochemical and Hf–Nd isotope data of Nanhua rift sedimentary and volcaniclastic rocks indicate a Neoproterozoic continental flood basalt provenance. Lithos 127, 427–440.

Wang, X.-C., Wilde, S.A., Li, Q.-L., Yang, Y.-N., 2015. Continental flood basalts derived from the hydrous mantle transition zone. Nat. Commun. 6, 1.

White, A.F., Brantley, S.L., 1995. Chemical weathering rates of silicate minerals: an overview. Rev. Mineral. Geochem. 31, 1–22.

Wignall, P.B., 2001. Large igneous provinces and mass extinctions. Earth-Sci. Rev. 53, 1–33.

Wingate, M.T.D., Giddings, J.W., 2000. Age and palaeomagnetism of the Mundine Well dyke swarm, Western Australia: implications for an Australia–Laurentia connection at 755 Ma. Precambrian Res. 100, 335–357.

Wingate, M.T.D., Campbell, I.H., Compston, W., Gibson, G.M., 1988. Ion microble U–Pb ages for Neoproterozoic basaltic magmatism in south-central Australia and implications for the break-up of Rodinia. Precambrian Res. 87, 135–159.

Yoshioka, H., Asahara, Y., Tojo, B., Kawakami, S., 2003. Systematic variations in C, O, and Sr isotopes and elemental concentrations in Neoproterozoic carbonates in Namibia: implications for glacial to interglacial transition. Precambrian Res. 124, 69–85.

Zhao, J.-H., Zhou, M.-F., 2007. Geochemistry of Neoproterozoic mafic intrusions in the Panzihua district (Sichuan Province, SW China): implications for subduction- related metasomatism in the upper mantle. Precambrian Res. 152, 27–47.